ISA
TRANSACTIONS®

ISA Transactions 44 (2005) 145–163

Design and analysis of controllers for a double inverted pendulum

Henrik Niemann,[a,*] Jesper Kildegaard Poulsen[b,†]

[a]*Ørsted-DTU, Automation, Technical University of Denmark, Building 326, DK-2800 Lyngby, Denmark*
[b]*Intentia Danmark A/S, Borupvang 5 D-E, DK-2750 Ballerup, Denmark*

(Received 25 November 2002; accepted 7 May 2004)

Abstract

A physical control problem is studied with the $\mathcal{H}_\infty$ and the μ methodology. The issues of modeling, uncertainty modeling, performance specification, controller design, and laboratory implementation are discussed. The laboratory experiment is a double inverted pendulum placed on a cart. The limitations in the system with respect to performance are the limitation in the control signal and the limitation of the movement of the cart. It is shown how these performance limitations will effect the design of $\mathcal{H}_\infty$ and μ controllers for the system. © 2005 ISA—The Instrumentation, Systems, and Automation Society.

Keywords: Modeling; $\mathcal{H}_\infty$ controller design; μ synthesis; Simulation; Controller implementation; Laboratory experiments

1. Introduction

The pendulum system is one of the classical examples used in connection with feedback control. The inverted single pendulum is a standard example in many text books dealing with classical as well as modern control. The reason is that the system is quite simple, nonlinear, and unstable. In connection with the classical control, the single inverted pendulum system has among other things been used to show that the system cannot be stabilized by using just a P controller. In spite of the fact that the system is unstable, the design of stabilizing controllers for the system can be done reasonably easy. However, this is not the case when considering the quite more complicated double inverted pendulum system. It is more complicated to design/tune stabilizing controllers for the system. Therefore more advanced controller architectures and advanced design methods need to be applied. This involved different types of model based controllers designed by using, e.g., $\mathcal{H}_2$ based methods, $\mathcal{H}_\infty$ based methods, and μ based methods.

A benchmark problem for robust controller design derived by Wei and Bernstein [1] has been described in a special issue in AIAA Journal of Guidance, Control, and Dynamic, Vol. 15, No. 5, 1992. The benchmark problem is a linear two-mass-spring system with uncertain masses and spring constant. Compared with the double inverted pendulum system, the linear benchmark problem is less complicated, but still a quite challenged design problem. A number of different design approaches has been applied on the linear benchmark problem, among them also $\mathcal{H}_\infty$ controller design and μ synthesis, see Refs. [2–7].

The main problem in the design of stabilizing controllers for the double inverted pendulum system is the tradeoff between robust stability and performance. This tradeoff is limited and there is not much space for reduction of the robustness to increase the performance of the system. The reason is the nonlinearities in the system together with the limitations/saturations in the system. The

**E-mail address:* hhn@oersted.dtu.dk
†*E-mail address:* jesper.k.poulsen@intentia.dk

Nomenclature

θ_1	angle between vertical and the lower arm
$\dot{\theta}_1$	angular velocity related to θ_1
θ_2	angle between vertical and the upper arm
$\dot{\theta}_2$	angular velocity related to θ_2
x_c	cart position
$\dot{x}_c$	velocity of the cart
i	motor current
U	reference voltage to motor/tacho system, control signal
r_c	cart position reference
M_{d_1}	torque disturbance on the joint on the lower arm
M_{d_2}	torque disturbance on the joint on the upper arm
M_{dm}	torque disturbance on the motor
n_1	noise signal in measuring θ_1
n_3	noise signal in measuring $\theta_3 = \theta_1 - \theta_2$
n_x	noise signal in the measuring of the cart position x_c
e_c	cart position error $r_c - x_c$

mass of cart	m	0.81 kg
length of track	l_t	1.34 m
mass of lower arm	m_1	0.548 kg
length of lower arm	l_1	0.535 m
length of lower arm from bottom to center of mass	l_{1cm}	0.355 m
inertia of lower arm around the lower joint	I_1	$2.678e^{-2}$ kg m^2
mass of upper arm	m_2	0.21 kg
length of upper arm	l_2	0.512 m
length of upper arm from bottom to center of mass	l_{2cm}	0.12 m
inertia of upper arm around the lower joint	I_2	$5.217e^{-3}$ kg m^2

limitations in the system are, e.g., maximal power to the motor (maximal acceleration of the cart), and maximal length of the track, to mention the two most important limitations. In spite of this limited tradeoff between robustness and performance of the system, it is possible to design controllers that can handle this tradeoff in a systematic way. Design methods such as, e.g., $\mathcal{H}_2$, $\mathcal{H}_\infty$, and μ based methods can be applied for handling this tradeoff in a systematic way.

This paper describes a complete design procedure for the design of advanced stabilizing controllers for the double inverted pendulum system together with an implementation of the controllers on a laboratory system. This leads to the following items that will be considered:

- system modeling,
- system analysis,
- uncertainty modeling,
- design problem formulation,
- controller design,
- analysis of the closed-loop system,
- implementation of controllers on a microcontroller,
- validation of the closed-loop system on the laboratory system.

Due to the lack of space, the first three items will only be considered briefly. A more detailed description of these parts can be found in Ref. [8]. This paper is organized as follows: In Section 2,

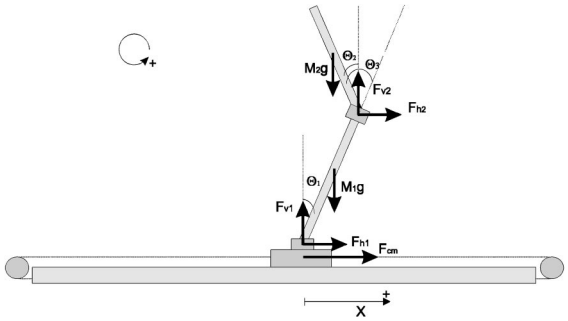

Fig. 1. Principal diagram of the double inverted pendulum system.

the double inverted pendulum system is briefly described, including a description of the model uncertainties and a formulation of performance conditions for the controller design problem. Controller designs are described in Section 3. Section 4 includes an analysis of the designed controllers derived in both the frequency domain as well as in the time domain. The laboratory experiments are described in Section 5 followed by a conclusion in Section 6.

2. Model of a double inverted pendulum

In the following, a short description of the double inverted pendulum system is given. Both the nominal as well as a real laboratory model are considered. A more detailed description can be found in Ref. [8]. The construction of the pendulum system is described in Ref. [9].

2.1. Description of the system

The double inverted pendulum system consists of a cart placed on a track, and two aluminum arms connected to each other. These are constrained to rotate within a single plane. The axis of the rotation is perpendicular to the direction of the motion of the cart. The cart is attached to the bottom of the pendulum, moving along a linear low friction track. The cart is moved by an exerting force by a servo motor. A principal structure of the pendulum system is shown in Fig. 1, where the forces acting on the system have been included.

A nonlinear model for the complete system can be derived by using Newton's second law and third law on every part of the system. A detailed description of the nonlinear model can be found in Ref. [8]. Based on this nonlinear model, a linear model can be derived by a linearization of the nonlinear model around the working point. The linear model Σ_G for the complete system can be described by the following state space description:

$$\Sigma_G : \begin{cases} \dot{x} = Ax + B_w w + B_u u \\ y = C_y x + D_{yw} w + D_{yu} u, \end{cases} \quad (1)$$

where x is the state, w is the exogenous inputs, u is the control input, and y is the measurement output. The linear model is of order 7 with the following states:

$$x = [\theta_1 \;\; \dot{\theta}_1 \;\; \theta_2 \;\; \dot{\theta}_2 \;\; x_c \;\; \dot{x}_c \;\; i]^T. \quad (2)$$

The exogenous input vector is given by

$$w = [r_c \;\; M_{d_1} \;\; M_{d_2} \;\; n_1 \;\; n_3 \;\; M_{dm} \;\; n_x]^T. \quad (3)$$

The measurement vector y is given by

$$y = [e_c \;\; \theta_1 \;\; \theta_3]^T. \quad (4)$$

The state space matrices in Eq. (1) are given in the Appendix.

The pendulum system is an unstable system with the following open-loop poles:

$$\text{poles} = \{0, \; -251, \; -7441, \; -6.4, \; 6.4, \; -4.1, \; 4.1\}.$$

2.2. Formulation of nominal design problem

Based on the system setup in Section 2.1, the following main conditions to the pendulum system can be formulated:

- The cart position has to be close to a given reference signal r_c, with limit cycles as small as possible. This means that the goal is to minimize $e_c = r_c - x_c$.
- The lower arm has to be as close as possible to vertical, while still allowing the cart to move. This means that the angle θ_1 is to be minimized.
- The upper arm is to be as close to vertical as possible, meaning that the angle θ_2 is minimized, which in terms of system outputs means that $\theta_1 - \theta_3$ is minimized.

This type of control problem is often referred to as a tracking problem, as in Ref. [10]. When designing a controller the performance and the bandwidth available have a major influent, and therefore it is important to include the controller signal U as an exogenous output. Selecting the signal U as an output gives the possibility to limit the bandwidth and gain of the designed controllers.

Since the motor system is an isolated closed-loop system it is not easy to influence its dynamics with the higher level controller. The only way to give the controller access to the motor system dynamics is to select one of its signals as an exogenous output. A good reason to select the current i as the output is that it is proportional to the generated motor torque.

The exogenous output vector is selected as

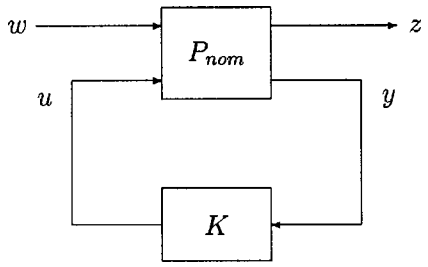

Fig. 2. The standard setup for design of feedback controllers.

$$z=\begin{bmatrix} e_c \\ \theta_1 \\ \theta_2 \\ U \\ i \end{bmatrix}. \tag{5}$$

When the exogenous outputs are included in the state space setup the nominal system Σ_P is defined by

$$\Sigma_P:\begin{cases} \dot{x}=Ax+B_w w+B_u u, \\ z=C_z x+D_{zw} w+D_{zu} u, \\ y=C_y x+D_{yw} w+D_{yu} u, \end{cases} \tag{6}$$

where the exogenous input w is defined in Section 2.1. The state space matrices are given in the Appendix.

This state space formulation can be put into the general control configuration as seen in Fig. 2, where

$$\begin{bmatrix} z \\ y \end{bmatrix}=P_{nom}\begin{bmatrix} w \\ u \end{bmatrix}.$$

2.3. Formulation of robust design problem

The model of the real system includes a number of uncertainties. These uncertainties can be split up into two groups:

- parameter uncertainty;
- neglected linear, nonlinear, and unmodeled dynamics uncertainty.

It is easy to identify a number of uncertain parameters. Some parameters are difficult or impossible to get a precise measure of, and other tend to vary as function of time, temperature, etc. The Coulomb friction is the main certain parameter in this system.

With respect to neglected dynamics, the pendulum system does have unmodeled dynamics like bearings, track inclination, and all kinds of high-frequency dynamics, etc. Further, the system includes also nonlinear elements/dynamics. The nonlinear dynamics appear from the sine and cosine functions in the nonlinear model. However, the system will only work with small angles, which will reduce the nonlinear effect from the sine and cosine functions.

From simulations, it was found that the system is especially sensitive to offsets on the angular measurements and in general any kind of disturbance on the measurements. Since it is not possible to make an uncertainty model of offsets, due to its nonlinear nature, it has been modeled as a general uncertainty. This implies that it will be reasonable to model the uncertainty as multiplicative output uncertainty. The multiplicative output uncertainty is described by

$$G_p=(I+W_o\Delta_o)G, \tag{7}$$

where the perturbation matrix Δ_o is given as either structured or unstructured and satisfies $\|\Delta_o\|_\infty \leqslant 1$ as in Ref. [10] and where W_o is a weight that indicates the relative error as function of frequency. An unstructured perturbation matrix is a matrix with complex numbers in all elements. A structured perturbation matrix is a block diagonal matrix with either complex or real elements, as

$$\Delta=\begin{bmatrix} \Delta_1 & & \\ & \ddots & \\ & & \Delta_i \end{bmatrix}.$$

All the important system uncertainties have been lumped into a simple uncertain block/blocks at the output of the system given by Eq. (7). The main uncertainty in this system is in relation with the dynamic of the two arms. Based on this, uncertainties have only been added to the two angle measurements θ_1 and θ_3. Based on a full nonlinear model, bounds on the uncertain blocks can then be derived based on a grid over the working area for the pendulum system to get the worst case uncertainties; see, e.g., Ref. [10].

However, these bounds cannot be applied directly in connection with design of robust controllers. It turns out that main limitation in the system is the length of the track together with the applied robust feedback controller that gives some bounds

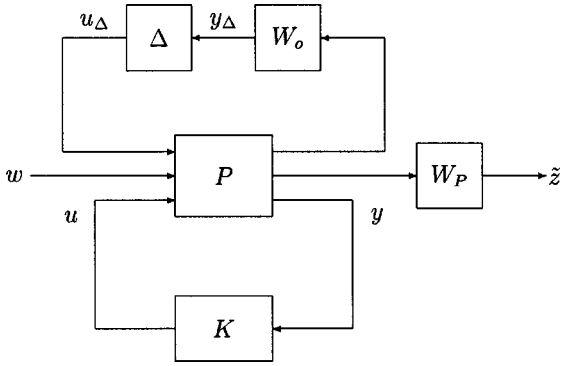

Fig. 3. The complete system setup for design of robust feedback controllers.

on the uncertainties for which the system can be stabilized. Based on this fact and for keeping the weight functions as simple as possible, the weight functions have been selected as constant weight functions. A full block complex perturbation with constant weight has been applied in connection with $\mathcal{H}_\infty$ design and diagonal complex perturbations in connection with μ synthesis.

3. Controller design

Four different controllers have been designed, three controllers by using the $\mathcal{H}_\infty$ design method directly and one controller by using the μ synthesis. The setup for the designs is based on the nominal setup described in Section 2.2 and the uncertain description for the system given in Section 2.3. Combining the nominal design setup with the uncertain model description gives the complete design setup shown in Fig. 3, where W_P is the weight matrix for the performance specification and W_o is the weight matrix for the multiplicative output uncertainty.

3.1. μ controller design

The μ controller is designed by using the DK iteration, Ref. [11]. Based on the performance specification in Section 2.2 and the model uncertainty description given in Section 2.3, we have that the two weight functions in Fig. 3 are given by

$$W_P = \mathrm{diag}(W_e, W_{\theta_1}, W_{\theta_2}, W_U, W_i),$$

$$W_o = \mathrm{diag}(W_{o_1}, W_{o_2}).$$

The selection of the weight matrices are based on the performance conditions.

The μ synthesis design method is selected because the uncertain description and the performance specification results in a structured design problem.

Based on the performance specifications given in Section 2.2 and the description of the model uncertainties in Section 2.3, weight functions for the μ synthesis design problem can be derived. The selection of the weight matrices is a tradeoff between selection of simple weight matrices and weight matrices, that are not conservative. In connection with this design problem, it has been desired to use only constant weights or first-order weights.

For the model uncertainty, the weight is selected as follows:

- The constant weight for the uncertain block is selected as $W_o = 0.05$.

The constant weight W_o represent a lumping of the nonlinear part of the system into a multiplicative output uncertain block.

The performance weights are related to the specifications of the cart position error e_c, the two angles θ_1 and θ_2, the control signal U, and the motor current i. As a help in connection with the selection of the weight matrices, the largest singular value for the open-loop transfer function from the exogenous input w to the exogenous output z have been derived and shown in Fig. 4. Based on the performance conditions and the amplitude plots shown in Fig. 4, the weight matrices are selected as follows:

- The weight on the cart position error e_c is a low-pass first-order weight. Since the reference tracking is not the most important control object, the weight is selected with a low cutoff frequency, thereby making it slow. The cutoff frequency has been selected to 1/30 rad/sec.
- From Fig. 4, it is seen that the largest singular value for both angles θ_1 and θ_2 is given as a kind of band-pass filter with a relative narrow band. This implies that changing the dynamic of the arms at either low or high frequencies will be quite expensive in terms of performance. The ideal controller would apply a lot of low-frequency performance in order to get the system to react on low-

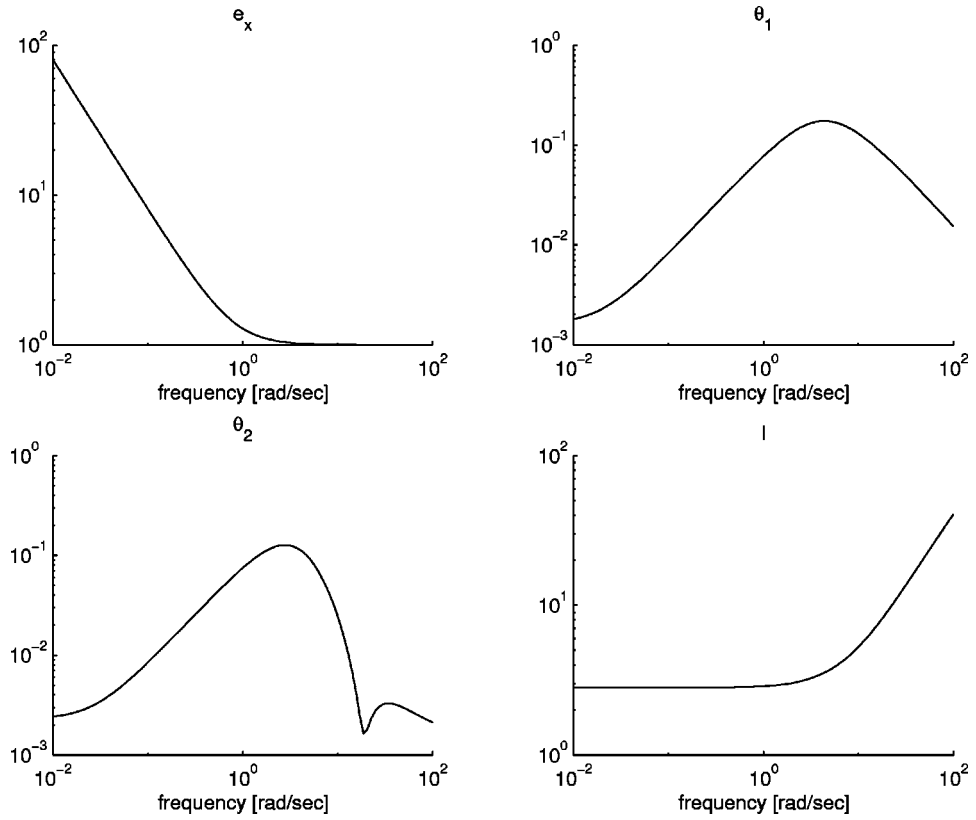

Fig. 4. Largest singular values for the transfer functions from the exogenous input w to the exogenous output z. The controller output U is not included since no controller has been designed yet.

frequency input signals, thereby making it easier to control. Another advantage with low-frequency performance is that the arms more easily can reject the Coulomb friction disturbance. To get more dynamic at low frequencies, we have to press down the singular value top to make the band wider. By selectiong a low-pass filter as the weight, the controller μ synthesis will press the peak down, and at the same time ensure that the controller does not try to apply all the performance to the low-frequency area. A cutoff frequency at 10 rad/sec has been selected for both weights.

- The weight on the control signal is applied to make sure that the controller does not apply performance in the high frequencies. The necessity for low-frequency limitation of the performance is especially clear after the selection of the angle weights. To ensure that the performance is put into the system at low frequencies instead of high frequencies, the weight have to be selected as a high-pass filter with a cutoff frequency above the important system dynamic. The cutoff frequency has been selected to 100 rad/sec.
- The weight on the dc-motor current is applied to control the cart acceleration. A small weight will make the cart react on smaller motor terminal voltage changes. Here the weight is selected to 1.0.

To summarize, the complete set of weight matrices for the μ controller design are given by

$$W_e = \frac{75}{30s+1}, \quad W_{\theta_1} = \frac{68}{s+10}, \quad W_{\theta_2} = \frac{40}{s+10},$$

$$W_U = 0.1 \times \frac{s+100}{0.01s+100}, \quad W_i = 1.0,$$

$$W_{o_1} = W_{o_2} = 0.05.$$

In Fig. 5, the dynamic weight functions given above are shown.

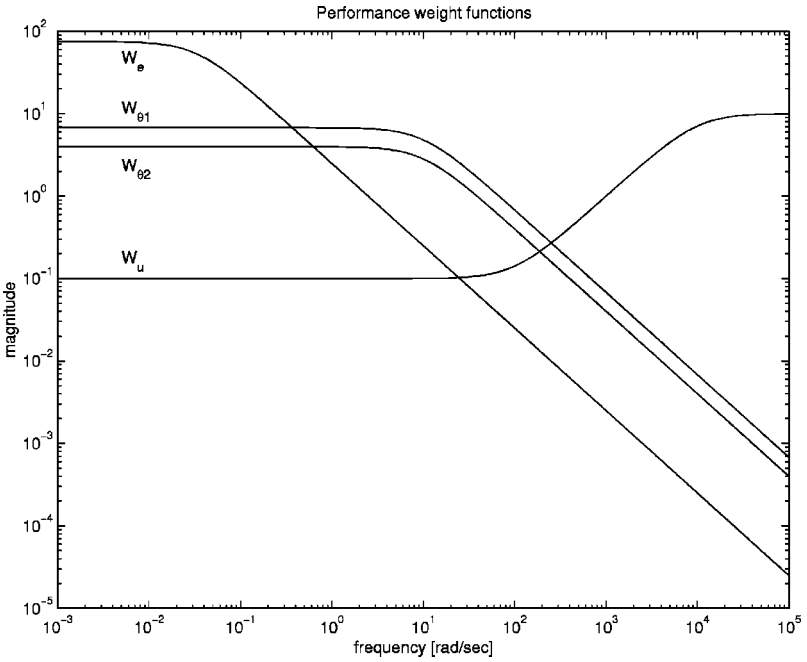

Fig. 5. The performance weight functions for the μ synthesis.

3.2. $\mathcal{H}_\infty$ controller design

Three $\mathcal{H}_\infty$ controllers are designed by using the standard $\mathcal{H}_\infty$ design method, described in, e.g., Ref. [11], and compared with the μ controller described in Section 3.1. Note that the diagonal structure in the uncertain block and in the performance block is not taken into account in the $\mathcal{H}_\infty$ controller design.

The weight matrices for the three $\mathcal{H}_\infty$ designs have been selected with respect to pure performance design (the $\mathcal{H}_\infty^1$ and the $\mathcal{H}_\infty^2$ controller) or with respect to a robust performance design (the $\mathcal{H}_\infty^\Delta$ controller). The difference between the first two designs is that the weight at the current i has been reduced by a factor 10 in the second design. This will result in a faster system but less robust against uncertainty in the system.

The weight matrices for the three different $\mathcal{H}_\infty$ controller designs have been selected as follows:

- $\mathcal{H}_\infty^1$ controller—the first $\mathcal{H}_\infty$ controller design, nominal design,

$$W_e=\frac{25}{50s+1},\quad W_{\theta_1}=\frac{50}{s+10},\quad W_{\theta_2}=\frac{45}{s+10},$$

$$W_U=0.1\times\frac{s+100}{0.01s+100},\quad W_i=0.1,\quad W_o=0.$$

- $\mathcal{H}_\infty^2$ controller—the second $\mathcal{H}_\infty$ controller design, nominal design,

$$W_e=\frac{25}{50s+1},\quad W_{\theta_1}=\frac{50}{s+10},\quad W_{\theta_2}=\frac{45}{s+10},$$

$$W_U=0.1\times\frac{s+100}{0.01s+100},\quad W_i=0.01,\quad W_o=0.$$

- $\mathcal{H}_\infty^\Delta$ controller—the third $\mathcal{H}_\infty$ controller design, robust design,

$$W_e=\frac{65}{50s+1},\quad W_{\theta_1}=\frac{50}{s+10},\quad W_{\theta_2}=\frac{45}{s+10},$$

$$W_U=0.1\times\frac{s+500}{0.01s+500},\quad W_i=0.1,$$

$$W_o=0.05.$$

The three controller designs based on the weight selection given above result in $\mathcal{H}_\infty$ controllers of order 11.

4. Controller analysis

The four different controllers will be analyzed in this section. The analysis is derived in both the frequency domain as well as in the time domain.

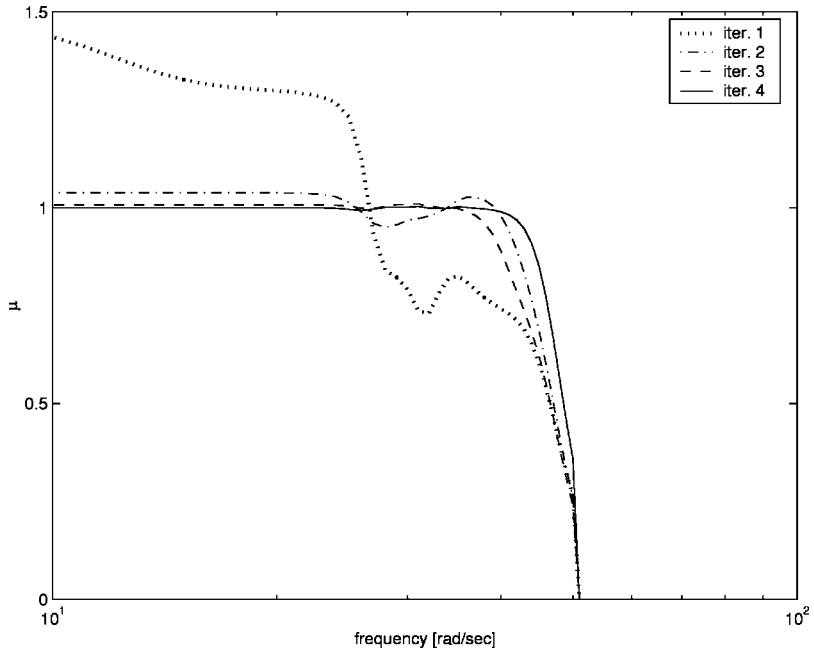

Fig. 6. The μ values for the four steps in the DK iteration.

4.1. μ controller

The μ value for the four iterations in the DK iteration is shown in Fig. 6. It is shown clearly in Fig. 6, that the μ value is reduced from the first iteration to the last iteration with a final value of μ below 1.

The four transfer functions between the uncertainty model input signal u_Δ and the uncertainty model output signal y_Δ when the μ controller is applied are shown in Fig. 7.

A simulation of the closed-loop system is shown in Fig. 8. From Fig. 8, it can be seen that the cart position reference tracking is slow. It does not settle around $x=0$ within the 5 sec of the simulation. The system is also very sensitive to the angles, showing large overshots but very fast settling time. The limit cycles are very small.

The initial conditions for the angles in the simulation are very small compared to the amplitude of the oscillations; this is not a trivial observation. It turns out that the selection of the initial start up angles are restricted in order for the controller to stabilize the system. By simulating the system a number of times with random generated initial start up angles it is possible to get an insight into the restriction on the sizes. The result is shown in Fig. 9.

As observed, the initial angles are very restricted. When the initial angles have the same sign, the pendulum is considerably easier to stabilize than when they have opposite signs. This is rather interesting in a practical sense, since the easiest way to hold the pendulum before starting the controller is to let the arms point in opposite directions.

It turns out that the final μ controller is of order 19 after four iterations. Therefore a model reduction is needed to reduce the order of the controller. The reduction of the controller is derived by using the optimal Hankel norm approximation, see, e.g., Ref. [10]. The result of the reduction of the controller order is shown in Fig. 10. A reduction of the controller order to order 6 or 7 does not have any serious effect on the performance of the system. A seventh order controller is implemented on the laboratory model.

4.2. $\mathcal{H}_\infty$ controllers

The four transfer functions between the uncertainty model input signal u_Δ and the uncertainty model output signal y_Δ when the $\mathcal{H}_\infty$ controllers are applied are shown in Fig. 11. As it can be seen from the figures, there is not much difference be-

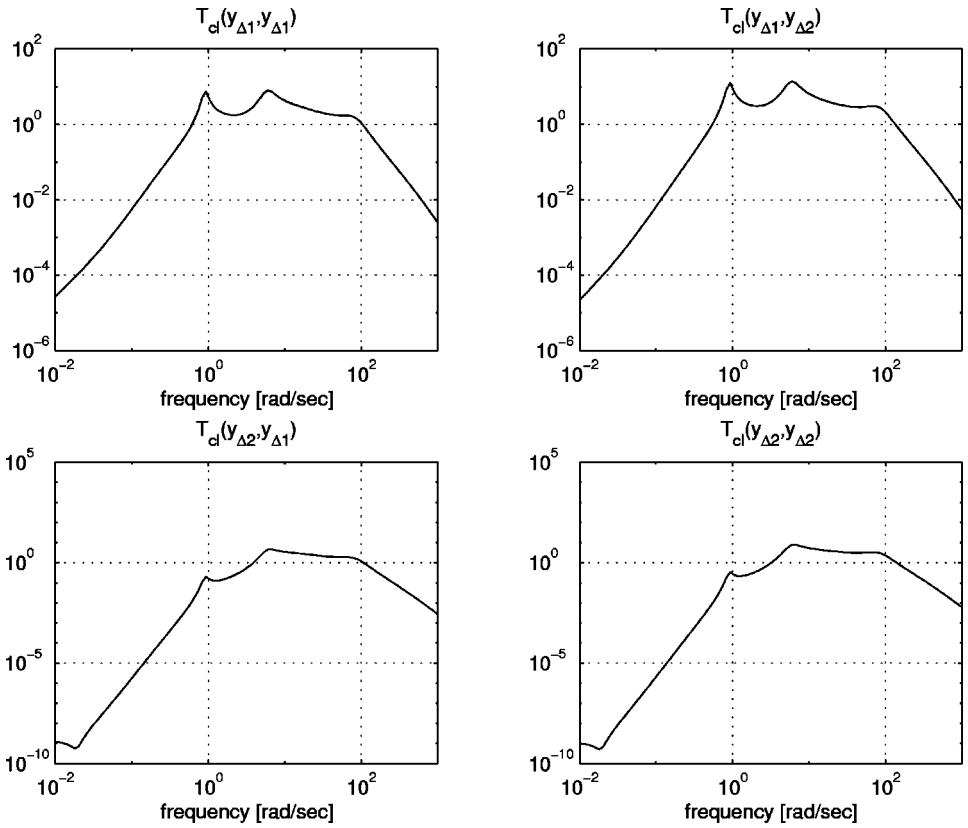

Fig. 7. Transfer functions for the angles between the uncertainty model input signal u_Δ and the uncertainty model output signal y_Δ when the μ controller is applied.

tween the closed-loop transfer functions when the three different $\mathcal{H}_\infty$ controllers are applied. Compared with the results for the μ controller in Fig. 7, there is not much difference.

A simulation of the closed-loop system is shown in Figs. 12 and 13. From Fig. 12, it can be seen that the $\mathcal{H}_\infty^\Delta$ controlled system has better reference tracking on the cart position than the other two. The $\mathcal{H}_\infty^2$ controlled system is very quickly stabilized, but with a offset error on the cart position that is slowly minimized. The $\mathcal{H}_\infty^1$ controlled system has the largest overshots due to the slower acceleration of the cart. This can also be seen in Fig. 13, where the $\mathcal{H}_\infty^1$ controlled system has the smallest control signal. This is in line with the selection of the weighting matrices, where the weight W_i has been reduced with a factor 10 for the $\mathcal{H}_\infty^2$ controller compared with the $\mathcal{H}_\infty^1$ controller.

Further, it can be seen that the signals do not settle at a fixed value, but oscillate with small amplitude. This oscillation is due to the nonstable nature of the system, combined with the Coulomb friction in the arm joints.

Compared the simulation results for the $\mathcal{H}_\infty$ controllers with the simulation for the μ controller shown in Fig. 8, no radical changes are observed. The μ-synthesis controller appears in no way to be superior in terms of this measure. So even though the uncertainty model is included, no increased robustness to nonlinearities or the startup problem is observed. The controllers are compared on the laboratory model in Section 5.

In line with the μ controller, a simulation of the initial angles from which the $\mathcal{H}_\infty$ controllers stabilize the system has been derived. The result is shown in Fig. 14. Compared with the μ controlled systems, the stability region for the $\mathcal{H}_\infty^\Delta$ controlled system is similar to the stability region for the μ controlled system. Using DK iteration has therefore not increased the initial stability region for the closed-loop system.

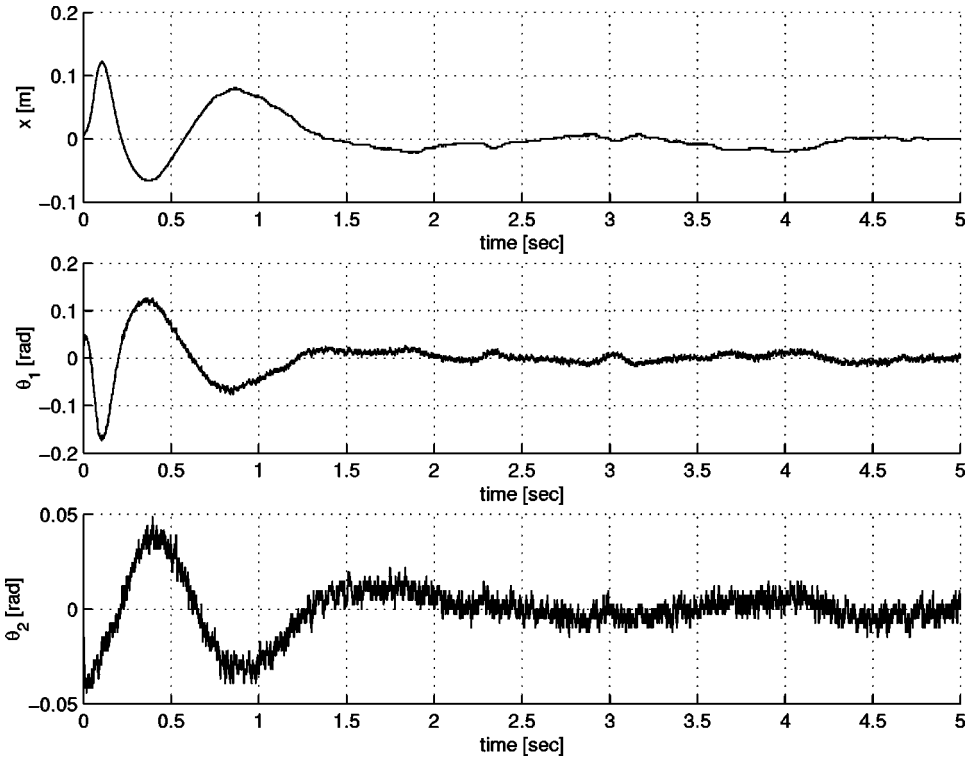

Fig. 8. Simulation of the nonlinear system with the μ controller. The initial conditions are $\theta_1 = 0.05$ rad and $\theta_2 = -0.04$ rad, similar to what would happen for the laboratory model.

An interesting observation is that the stability regions are in line with the design of the different controllers. The $\mathcal{H}_\infty^2$ controller, optimized with respect to performance, has the smallest stability region, whereas the $\mathcal{H}_\infty^\Delta$ controller, optimized with respect to robust stability, has the largest stability region. It should be pointed out in connection with this observation that this is not a proof of the stability regions for the closed-loop systems.

In the next section, the $\mathcal{H}_\infty$ controllers are implemented as full orders controllers on the real system. However, the controllers can be reduced to order 7 with only a minor reduction of the performance of the $\mathcal{H}_\infty$ controllers.

5. Laboratory experiments

The four controllers have been implemented as discrete-time controllers on a microcontroller. The microcontroller used here is a Motorola 68040 computer running with the real time operating system OS9. The microcontroller has an interface card with multiple 12-bit AD/DA converters. The converters have a range of ± 5 V. A sampling period of $T_s = 2$ msec has been used. Fig. 15 shows the principal wiring of the whole system.

The controller is implemented in Simulink. The A/D inputs and the D/A outputs are implemented in the Simulink library. Using the Real-Time Workshop (RTW) Toolbox, the Simulink model is the compiled in to OS9 executable code.

The continuous-time controller is transformed into an equivalent discrete-time controller by using the bilinear Tustin transformation given by

$$s = \frac{2}{T_s}\frac{z-1}{z+1}.$$

The result of the laboratory experiments is shown in Figs. 16–19 for the μ controller and the three different $\mathcal{H}_\infty$ controllers. Note that in all four cases, the system is started up with very small angles, i.e., $\theta_1 \approx 0$ and $\theta_2 \approx 0$.

5.1. Comparing the controllers

It is natural to make a comparison of the four different controllers on the real system. From the

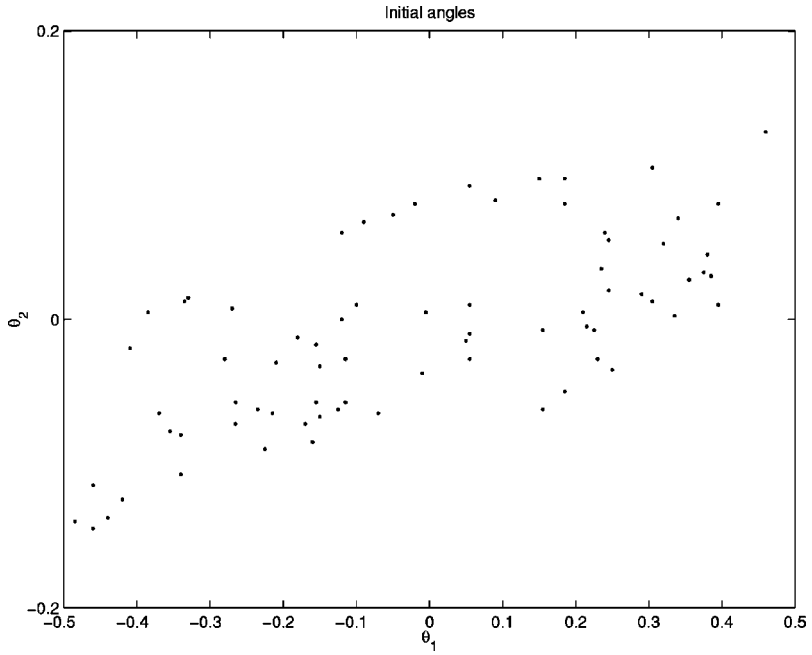

Fig. 9. Simulation of the initial angles from which the μ controller can stabilize the system. The contour formed by the dots shows the area from where the closed-loop system can be started in order to be stabilized.

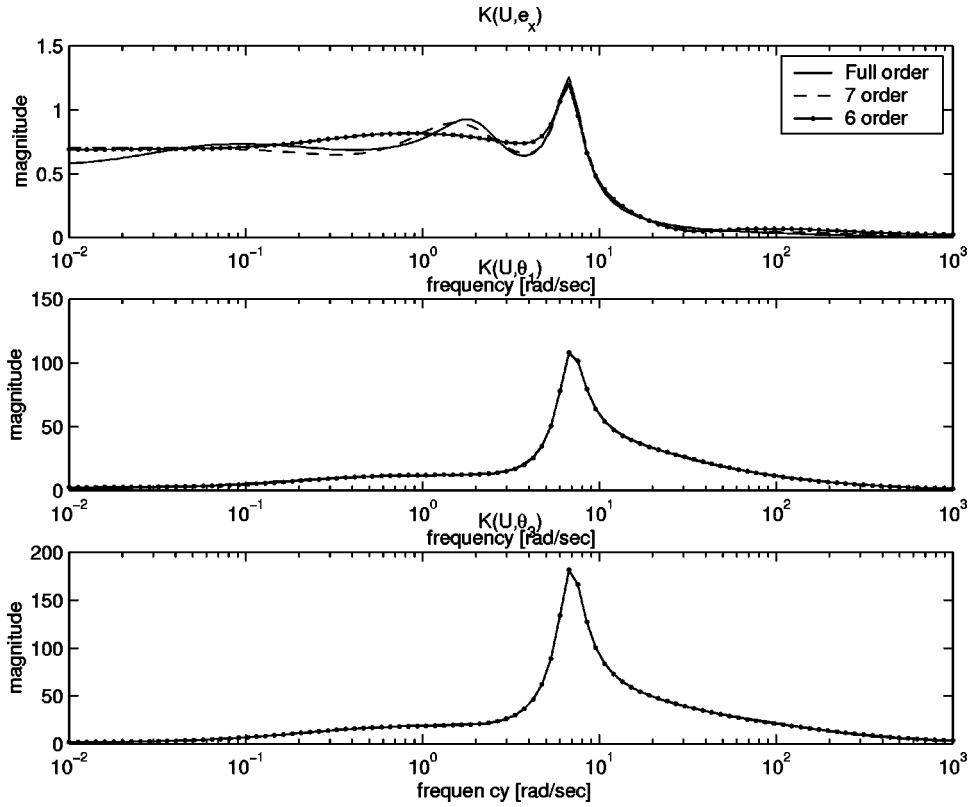

Fig. 10. Controller transfer functions for the full order controller and the two reduced controllers.

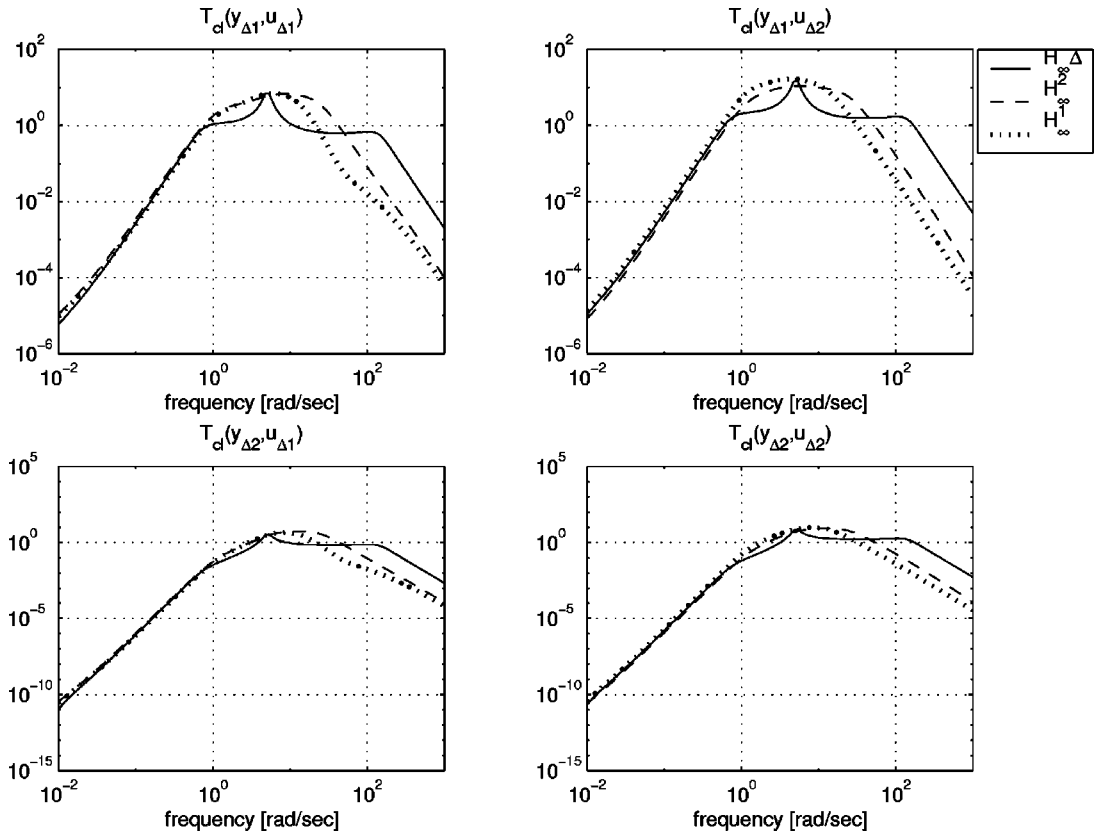

Fig. 11. Transfer functions for the angles between the uncertainty model input signal u_Δ and the uncertainty model output signal y_Δ.

simulations, it is known that there is not much difference between the four controllers.

The laboratory experiments for the four different controllers are shown in Figs. 16–19. These laboratory results show again only a minor difference between the performance of four different controllers. For a more systematic comparison of the controllers, let us define maximal peak value of an output variable, maximal peak value of a steady-state output variable, and the dominated frequency of the limit cycle of an output variable in steady-state response, given by

$$\begin{aligned} &\mathrm{Max}_p: \text{ maximal peak value of an output variable,}\\ &\mathrm{Max}_{ss}: \text{ maximal peak value of an output variable in steady state,}\\ &\mathrm{Freq}: \text{ dominated frequency of the limit cycle.} \end{aligned} \tag{8}$$

It should be pointed out that the maximal peak value Max_p depends strongly on the initial condition for the pendulum system. The initial conditions for the selected laboratory results shown in Figs. 16–19 are quite similar, however, they are not equal. This means that the maximal peak value Max_p should be used with care in connection with comparison of the different controllers. Further, the maximal peak value Max_{ss} and the dominated frequency of the limit cycle Freq are based on the last 10 sec of the laboratory experiments. The values of the three parameters for the four different feedback controllers are given in Tables 1–4.

It is not easy to compare the four different controllers from either the simulation results or from the laboratory experiments. There is not much difference between the four controllers.

The results of the laboratory experiments in Figs. 16–19 show that the $\mathcal{H}_\infty^2$ controller is quite better than the other controllers. However, the experiments do not show the real picture of the four

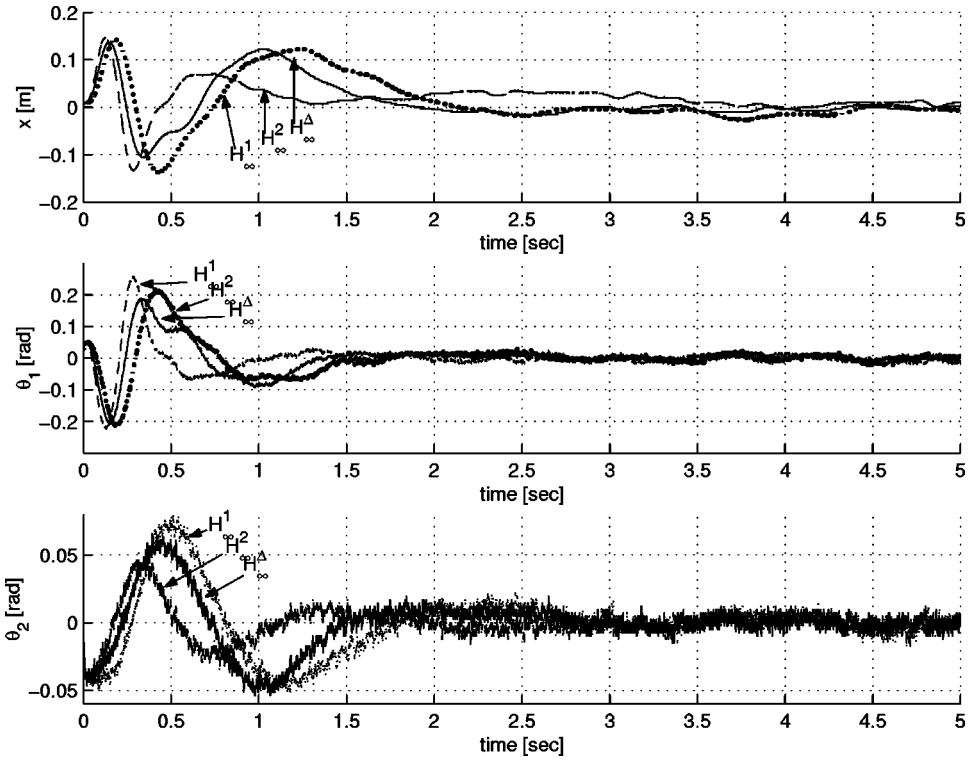

Fig. 12. Simulation of the nonlinear system with the three $\mathcal{H}_\infty$ controllers. The initial conditions are $\theta_1 = 0.05$ rad and $\theta_2 = -0.04$ rad, similar to what would happen for the laboratory model.

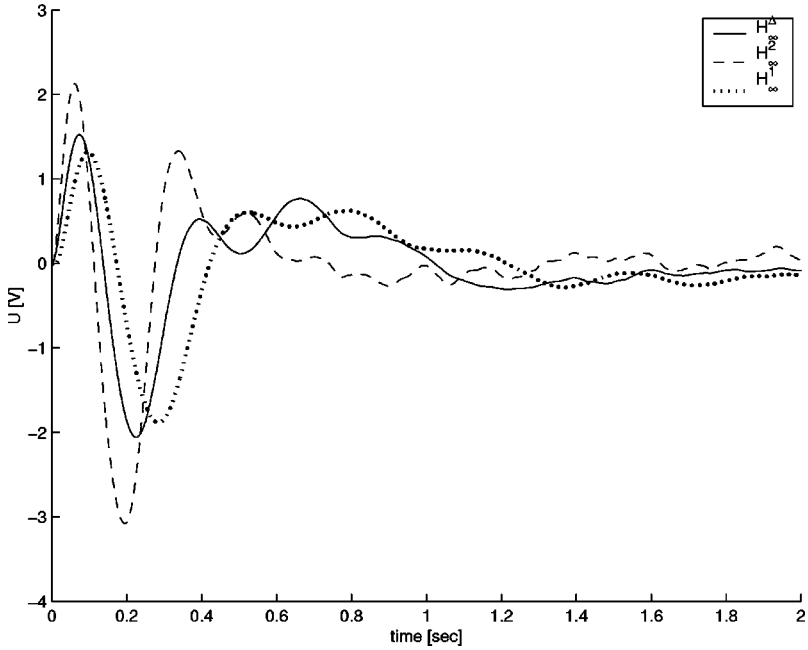

Fig. 13. Simulation of controller output signal U.

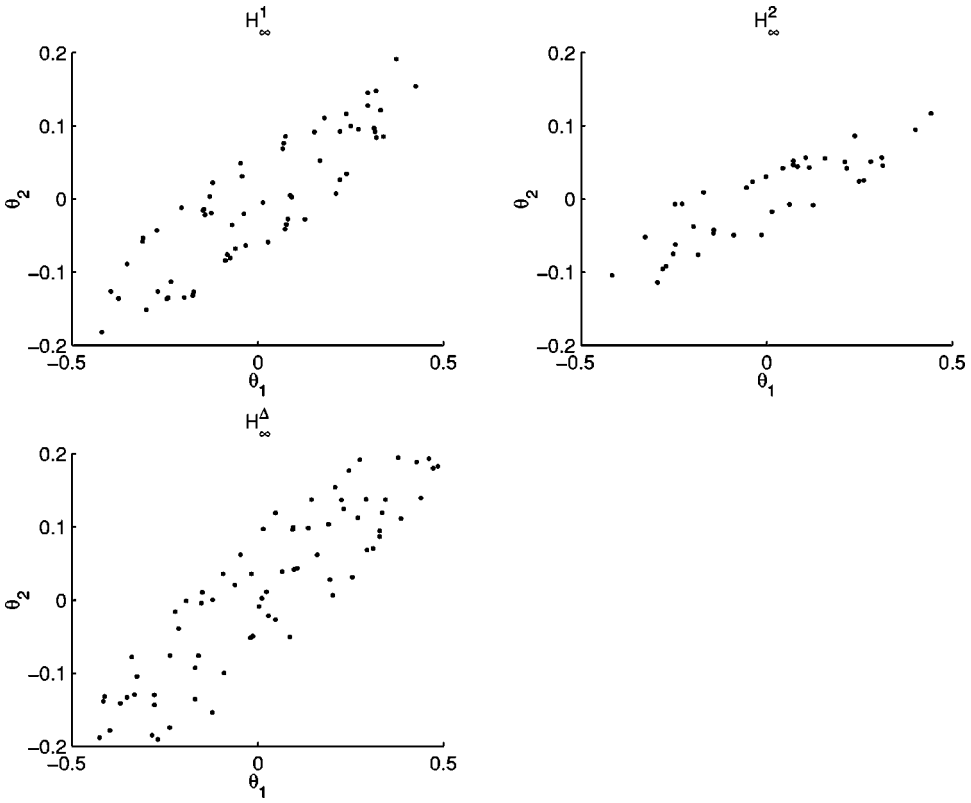

Fig. 14. Simulation of the initial angles from which the controllers can stabilize the system. The contour formed by the dots shows the area from where the closed-loop system can be started in order to be stabilized.

different closed-loop systems. It is very difficult to show the robustness of the four closed-loop systems through experiments. From Figs. 16–19, it is clear that the closed-loop system based on the $\mathcal{H}_\infty^2$ controller performs best. On the other hand, this system is also the most difficult system of the four systems to start up. This is in line with the simulation results shown in Fig. 14. Here it was shown that the $\mathcal{H}_\infty^2$ controlled system has the smallest initial stability region. Equivalently, the $\mathcal{H}_\infty^\Delta$ controlled system is much easier to start up, which is in line with Fig. 14. The performance of the closed-loop system is, on the other hand, reduced compared with the $\mathcal{H}_\infty^2$ controlled system. These results show the tradeoff between performance and robustness.

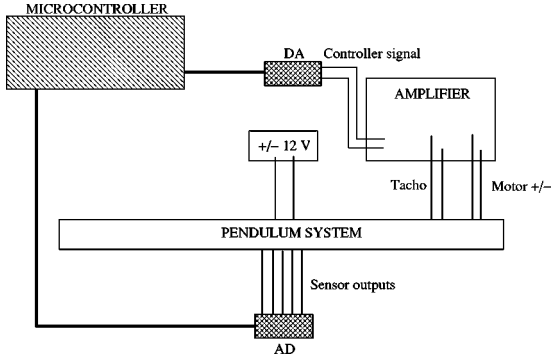

Fig. 15. Drawing showing the principal wiring of the whole system.

The μ controlled system has a quite good performance, see Fig. 16, and the robustness of the closed-loop system is also reasonable, see, e.g., Fig. 9. The μ controlled system seems to be a little better than the $\mathcal{H}_\infty^\Delta$ controlled system with respect to both performance and robustness. However, the tracking of the cart position is quite slow for the μ controlled system compared with the performance of the other closed-loop systems.

Comparing the controllers from Tables 1–4, it is shown very clearly the difference between the two robust controllers (μ and $\mathcal{H}_\infty^\Delta$ controller) and the two controllers optimized with respect to the per-

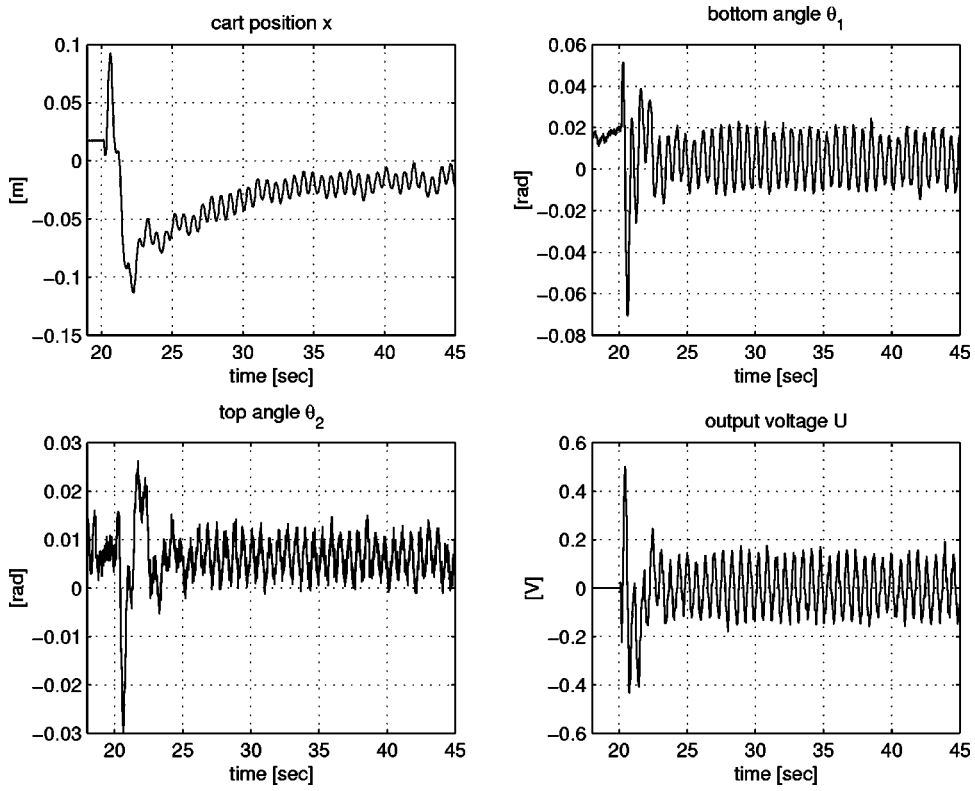

Fig. 16. Sampled data from laboratory model, running with the μ controller.

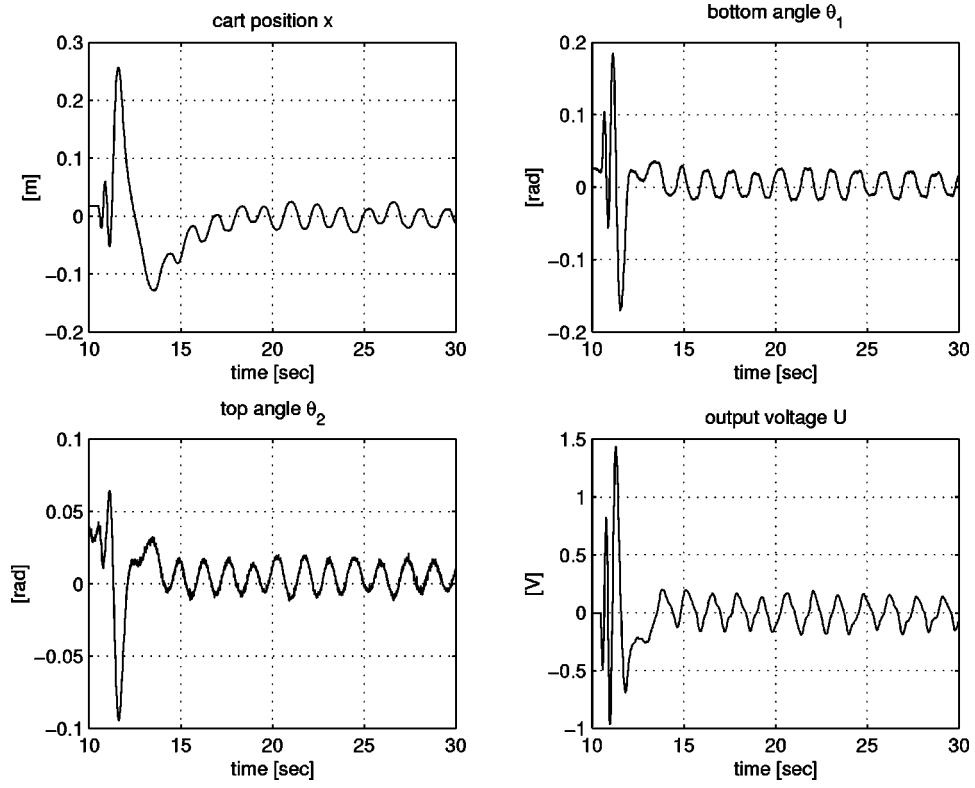

Fig. 17. Sampled data from laboratory model, running with the $\mathcal{H}_\infty^1$ controller.

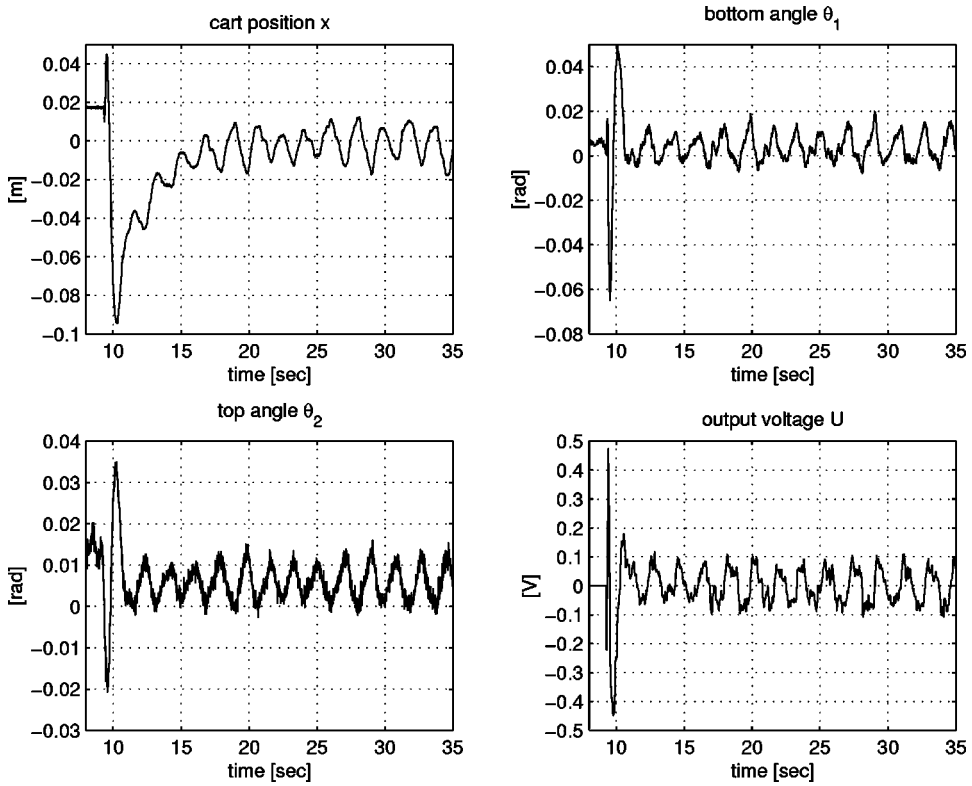

Fig. 18. Sampled data from laboratory model, running with the $\mathcal{H}_\infty^2$ controller.

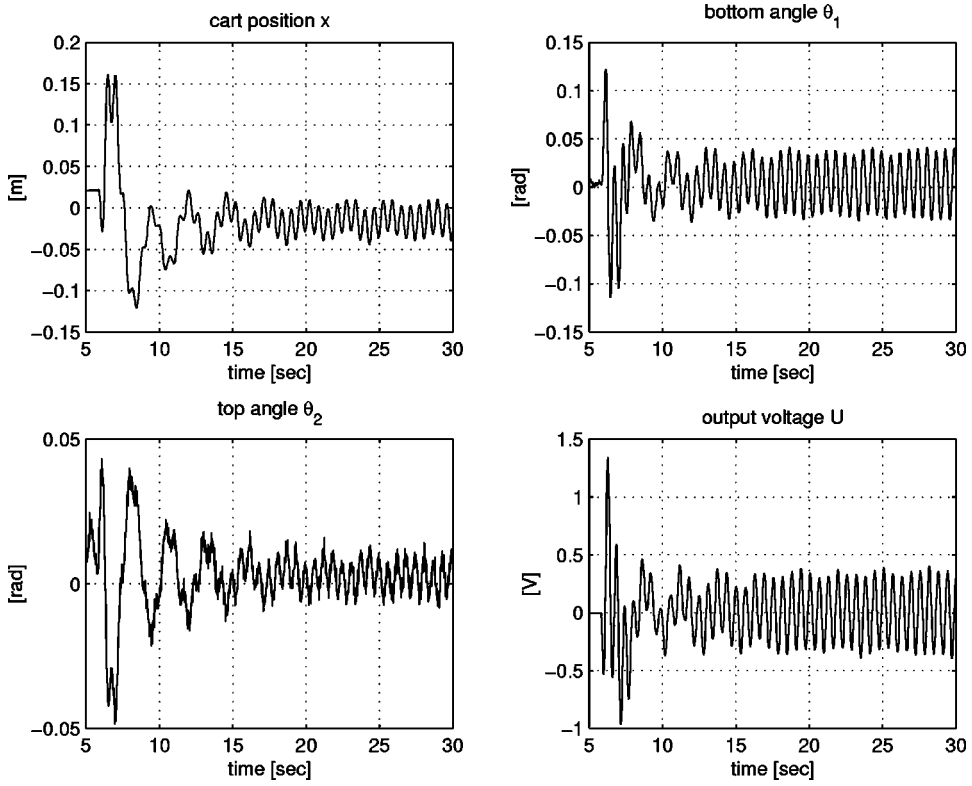

Fig. 19. Sampled data from laboratory model, running with the $\mathcal{H}_\infty^\Delta$ controller.

Table 1
Values for the μ controller.

Variable	Max_p	Max_{ss}	Freq
x	0.13 m	0.0095 m	
θ_1	0.05 rad	0.016 rad	9.6 rad/sec
θ_2	0.03 rad	0.0063 rad	
U	0.5 V	0.16 V	

Table 3
Values for the $\mathcal{H}_\infty^2$ controller.

Variable	Max_p	Max_{ss}	Freq
x	0.095 m	0.013 m	
θ_1	0.065 rad	0.013 rad	3.4 rad/sec
θ_2	0.035 rad	0.008 rad	
U	0.48 V	0.095 V	

formance ($\mathcal{H}_\infty^1$ and $\mathcal{H}_\infty^2$ controller). There is a factor 2.5 between the dominated frequencies of the limit cycles for the $\mathcal{H}_\infty^1$, $\mathcal{H}_\infty^2$ controllers and the μ, $\mathcal{H}_\infty^\Delta$ controllers. Further, comparing the maximal peak values Max_p and Max_{ss} for the μ controller and for the $\mathcal{H}_\infty^2$ controller, the values are almost identical. Only the maximal value of the control signal is a factor 1.6 larger for the μ controller than for the $\mathcal{H}_\infty^2$ controller.

Comparing the $\mathcal{H}_\infty^1$ and $\mathcal{H}_\infty^2$ controllers based on Tables 2 and 3, the $\mathcal{H}_\infty^2$ controller turns out to be the controller with the best performance. It is important to note that also the controller signal is smaller for the $\mathcal{H}_\infty^2$ controller compared with the $\mathcal{H}_\infty^1$ controller. Due to the reduced weight on the control signal in the design of the $\mathcal{H}_\infty^2$ controller, it was expected that the maximal values of the control signal was increased compared with the $\mathcal{H}_\infty^1$ controller.

Comparing the two robust controllers, i.e., the μ and the $\mathcal{H}_\infty^\Delta$ controller, based on Tables 1 and 4, it is shown that the μ controller has a marginally better performance than the $\mathcal{H}_\infty^\Delta$ controller. It is only comparing the maximal peak value of the control signal where the μ controller is much better that the $\mathcal{H}_\infty^\Delta$ controller.

6. Conclusion

A complete design and implementation of controllers for an unstable system has been described in this paper. A linear model of a double inverted pendulum system together with a description of the model uncertainties has been derived. A complete nonlinear model has been implemented in Simulink for use in connection with simulation of the system. Four different controllers have been designed by using the $\mathcal{H}_\infty$ and the μ synthesis methods. Finally, the designed controllers have been implemented on a microcontroller for laboratory experiments.

The four designed controllers have been validated both by simulation and calculation of various transfer functions as well as by laboratory experiments. In both the simulation as well as in the laboratory experiments, the tradeoff between the performance of the closed-loop system and robustness was shown. However, the tradeoff between performance and robustness for this system is very limited. The unstable double inverted pendulum system needs to be stabilized with a certain stability margin, else it is impossible to start the laboratory system up. This leaves only a minor freedom for the tradeoff between performance and robustness.

Appendix: System matrices

The system matrices in Eqs. (1) and (6) are given in the following:

Table 2
Values for the $\mathcal{H}_\infty^1$ controller.

Variable	Max_p	Max_{ss}	Freq
x	0.26 m	0.025 m	
θ_1	0.18 rad	0.019 rad	4.1 rad/sec
θ_2	0.096 rad	0.015 rad	
U	1.43 V	0.2 V	

Table 4
Values for the $\mathcal{H}_\infty^\Delta$ controller.

Variable	Max_p	Max_{ss}	Freq
x	0.16 m	0.02 m	
θ_1	0.12 rad	0.03 rad	9.9 rad/sec
θ_2	0.05 rad	0.0096 rad	
U	1.35 V	0.33 V	

$$A = \begin{bmatrix} 0 & 1 & 0 & 0 & 0 & 0 & 0 \\ 28.88 & 0 & -3.073 & 0 & 0 & 0 & -3.767 \\ 0 & 0 & 0 & 1 & 0 & 0 & 0 \\ -37.426 & 0 & 34.980 & 0 & 0 & 0 & 0.357 \\ 0 & 0 & 0 & 0 & 0 & 1 & 0 \\ -3.211 & 0 & 0.025 & 0 & 0 & 0 & 1.899 \\ 0 & 0 & 0 & 0 & 0 & -1.305e^{6} & -7.692e^{3} \end{bmatrix},$$

$$B_w = \begin{bmatrix} 0 & 0 & 0 & 0 & 0 & 0 & 0 \\ 0 & 0.004 & -0.005 & 0 & 0 & 10.656 & 0 \\ 0 & 0 & 0 & 0 & 0 & 0 & 0 \\ 0 & -0.005 & -0.057 & 0 & 0 & -1.010 & 0 \\ 0 & 0 & 0 & 0 & 0 & 0 & 0 \\ 0 & -0.004 & 0 & 0 & 0 & -5.370 & 0 \\ 0 & 0 & 0 & 0 & 0 & 0 & 0 \end{bmatrix},$$

$$B_u = \begin{bmatrix} 0 \\ 0 \\ 0 \\ 0 \\ 0 \\ 0 \\ 1.045e^{6} \end{bmatrix},$$

$$C_z = \begin{bmatrix} 0 & 0 & 0 & 0 & -1 & 0 & 0 \\ 1 & 0 & 0 & 0 & 0 & 0 & 0 \\ 0 & 0 & 1 & 0 & 0 & 0 & 0 \\ 0 & 0 & 0 & 0 & 0 & 0 & 0 \\ 0 & 0 & 0 & 0 & 0 & 0 & 1 \end{bmatrix},$$

$$D_{zw} = \begin{bmatrix} 1 & 0 & 0 & 0 & 0 & 0 & -5.0e^{-4} \\ 0 & 0 & 0 & 1.6e^{-3} & 0 & 0 & 0 \\ 0 & 0 & 0 & 0 & 1.6e^{-3} & 0 & 0 \\ 0 & 0 & 0 & 0 & 0 & 0 & 0 \\ 0 & 0 & 0 & 0 & 0 & 0 & 0 \end{bmatrix},$$

$$D_{zu} = \begin{bmatrix} 0 \\ 0 \\ 0 \\ 1 \\ 0 \end{bmatrix},$$

$$C_y = \begin{bmatrix} 0 & 0 & 0 & 0 & -1 & 0 & 0 \\ 1 & 0 & 0 & 0 & 0 & 0 & 0 \\ -1 & 0 & 1 & 0 & 0 & 0 & 0 \end{bmatrix},$$

$$D_{yw} = \begin{bmatrix} 1 & 0 & 0 & 0 & 0 & 0 & -5.0e^{-4} \\ 0 & 0 & 0 & 1.6e^{-3} & 0 & 0 & 0 \\ 0 & 0 & 0 & 0 & 1.6e^{-3} & 0 & 0 \end{bmatrix},$$

$$D_{yu} = \begin{bmatrix} 0 \\ 0 \\ 0 \end{bmatrix}.$$

References

[1] Wie, B. and Bernstein, D., Benchmark problems for robust control design. J. Guid. Control Dyn. **15**, 1057–1059 (1992).

[2] Adams, R. and Banda, S., Combined linear quadratic gaussian and H_∞ control of a benchmark problem. J. Guid. Control Dyn. **15**, 1134–1139 (1992).

[3] Chiang, R. and Safonov, M., H_∞ synthesis using bilineare pole shifting transform. J. Guid. Control Dyn. **15**, 1111–1117 (1992).

[4] Byrns, E., Jr. and Calise, A., Loop transfer recovery approach to H_∞ design for the coupled mass benchmark problem. J. Guid. Control Dyn. **15**, 1118–1124 (1992).

[5] Braatz, R. and Morari, M., Robust control for a noncollocared spring-mass system. J. Guid. Control Dyn. **15**, 1103–1110 (1992).

[6] Wang, Y., Shieh, S., and Sunkel, J., Observer based robust H_∞ control laws for uncertain linear systems. J. Guid. Control Dyn. **15**, 1125–1133 (1992).

[7] Wie, B., Liu, Q., and Byun, K., Robust H_∞ control synthesis method and its application to benchmark problems. J. Guid. Control Dyn. **15**, 1140–1148 (1992).

[8] Poulsen, J. K., Master's thesis, Automation, Ørsted-DTU, Technical University of Denmark, DK-2800 Lyngby, Denmark, 2001.

[9] Luther, J., Master's thesis, Department of Automation, Technical University of Denmark, DK-2800 Lyngby, Denmark, 1997.

[10] Skogestad, S. and Postlethwaite, I., Multivariable Feedback Control—Analysis and Design. John Wiley & Sons, Chichester, UK, 1996.

[11] Zhou, K., Doyle, J., and Glover, K., Robust and Optimal Control. Prentice Hall, Upper Saddle River, NJ, 1995.

Henrik Niemann was born in Slagelse, Denmark, January 4, 1961. He received the M.Sc. degree in mechanical engineering in 1986 and the Ph.D. degree in 1988 from Technical University of Denmark. From 1988 to 1994 he had a research position in control engineering at Technical University of Denmark. In 1994, he joined the Ørsted-DTU, Technical University of Denmark as Associate Professor in control engineering. From 1997 to 1998, he was visiting professor at Australian National University, Camberra, Australia. His research interests includes robust control, sampled-data systems, fault diagnosis, and fault tolerant control for linear and nonlinear systems.

Jesper Kildegaard Poulsen received the M.Sc. degree in electrical engineering in 2001 from Technical University of Denmark with special in robust control. Since 2003, he has been working at Intentia Danmark A/S in Denmark.